Accounting for saturation in conformal mapping modeling of a permanent magnet synchronous machine

Martin Hafner, David Franck and Kay Hameyer
Institute of Electrical Machines, RWTH Aachen University, Aachen, Germany

Abstract

Purpose – In the electromagnetic field simulation of modern servo drives, the computation of higher time and space harmonics is essential to consider appearing torque pulsations, radial forces and ripple torques. The purpose of this paper is to propose a method to cover the effect of saturation on the armature flux density within conformal mapping (CM) by an finite element (FE) re-parameterization.

Design/methodology/approach – Field computation by CM techniques is a time-effective method to compute the radial and tangential field components, but it generally neglects the effect of saturation.

Findings – This paper presents a method to re-parameterize the CM approach by single FE computations so as to consider saturation in the model over a wide operation range of the electrical drive.

Practical implications – The proposed method is applied to a surface permanent magnet synchronous machine, and compared to numerical results obtained by finite element analysis (FEA).

Originality/value – The paper shows that an accuracy similar to that of FE simulations can be obtained with still the low-computation time that is the characteristic of analytical models.

Keywords Magnetic fields, Modelling, Electrical machines, Simulation, Conformal mapping, Air-gap permeance, Permanent-magnet motors, Design methodology, Air-gap field

Paper type Research paper

1. Introduction

The design of electrical machines is routinely done by means of virtual prototyping nowadays, in order to reduce costs and shorten the time-to-market. Besides finite element analysis (FEA), which is computationally expensive, analytical models are also used to obtain a quick first approximation of the machine's behavior. Conventional analytical models usually focus on the determination of the fundamental air-gap flux density. Consequently, the effect of air-gap field harmonics on the main machine characteristics, such as back electromotive force, cogging and load torques, as well as the impact of geometry variations on those quantities, are neglected. In Hafner *et al.* (2009), the analytic conformal mapping (CM) method in frequency domain for permanent magnet synchronous machines (PMSM) is proposed and applied. The comparison with standard non-linear FEA shows that it gives a good approximation of the air-gap flux distribution, even if minor saturation occurs at local positions. Field harmonics and torque are in good agreement up to nominal current, but start to diverge in current overload situation. In this paper, a method is proposed to cover the effect of saturation on the armature flux density within CM by an finite element (FE) re-parameterization.

COMPEL: The International Journal for Computation and Mathematics in Electrical and Electronic Engineering
Vol. 30 No. 3, 2011
pp. 916-928

0332-1649
DOI 10.1108/03321641111110889

2. Standard conformal mapping

The air-gap field computation by CM is generally obtained from the solution of a linear Laplace problem, assuming the magnetic core has an infinite permeability. Since this system is linear, the field excitation by magnets and coils, as well the influence of the slotting, can be modeled individually.

Assuming first a slotless stator, the two-dimensional (2D) field $\vec{B}(\Theta)$ at a certain coordinate angle Θ in the air gap, $\Theta \in [0, 2\pi[$, consists of a radial flux density $B_r(\Theta)$ and a tangential flux density $B_\varphi(\Theta)$:

$$\vec{B}(\Theta) = B_r(\Theta) \cdot \vec{e}_r + B_\varphi(\Theta) \cdot \vec{e}_\varphi. \tag{1}$$

The angle dependent quantities $B_r(\Theta)$ and $B_\varphi(\Theta)$, can be expanded into a Fourier series:

$$\vec{B}(\Theta) = \sum_{n=0}^{\infty} \left(B_{r,n} \cdot \vec{e}_r + B_{\varphi,n} \cdot \vec{e}^{\,\varphi} \right) e^{jnp\Theta}, \tag{2}$$

where n is the frequency order and p the number of pole pairs. In this representation of the air-gap field, the Fourier coefficients $B_{r,n}$ and $B_{\varphi,n}$ are the solution of a linear Laplace problem with magnets and a slotless stator depending on the magnetization type (Zhu and Howe, 1993; Zhu *et al.*, 2002; Hanselman, 2003). The field at a certain instance of time t due to rotor movement is given by:

$$\vec{B}(t) = \vec{B} \cdot e^{j\omega_r t} \tag{3}$$

where ω_r is the angular speed of the rotor.

Stator slotting significantly influences the magnetic field distribution. It is standardly modeled by "permeance functions". These 2D permeance functions $\vec{\lambda}$ consider the radial and tangential impact of slotting on the slotless field distribution and can be obtained by Schwarz-Christoffel transformations (Zarko *et al.*, 2006, 2008). Correlating the field distribution with slotting, ${}^{s}\vec{B}(t)$, with the field without slotting (equation (3)), yields the vectorial permeance $\vec{\lambda}$:

$${}^{s}\vec{B}(t) = \vec{\lambda}^{*} \cdot \vec{B}(t) \tag{4}$$

$$\vec{\lambda}^{*} = \begin{pmatrix} \lambda_r & \lambda_\varphi \\ -\lambda_\varphi & \lambda_r \end{pmatrix}. \tag{5}$$

The magnetic field distribution due to a current in a single slot, assuming an infinite slot depth and an infinite permeability in a slotless stator, can be obtained analytically by three successive CMs (Binns, 1963), named current Ansatz function. According to the stator winding scheme, a flux distribution ${}^{b}\vec{B}$, in function of the effective number of winding turns and the coil current, representing the flux distribution per phase can be found from that. The overall armature field ${}^{a}\vec{B}(t)$ is given by:

$$ {}^{a}\vec{B}(t,I) = \begin{pmatrix} {}^{p}\vec{B}\left(\sqrt{2}Ie^{j\omega_s t+0^\circ}\right) \\ {}^{p}\vec{B}\left(\sqrt{2}Ie^{j\omega_s t+120^\circ}\right) \\ {}^{p}\vec{B}\left(\sqrt{2}Ie^{j\omega_s t+240^\circ}\right) \end{pmatrix} \cdot \begin{pmatrix} e^{j\phi_q+0^\circ} \\ e^{j\phi_q+120^\circ} \\ e^{j\phi_q+240^\circ} \end{pmatrix}, \tag{6} $$

where the angle ϕ_q defines the relative phase orientation to the quadrature axis of the machine and ω_s is the stator current angular frequency. Owing to the governing equation of the current Ansatz function in Binns (1963), the impact of $\vec{\lambda}$ is already considered in the definition of ${}^{p}\vec{B}$. We shall in the sequel systematically omit the arguments Θ and t and retain only the argument I for all quantities that are current dependent. We shall also label the quantities obtained by the CM approach with a *CM* exponent. The overall air-gap field by following the procedure explained above is thus defined as:

$$ {}^{g}\vec{B}^{CM}(I) = {}^{a}\vec{B}^{CM}(I) + {}^{s}\vec{B}^{CM}. \tag{7} $$

3. Saturation in conformal mapping

The considered PMSM is identical to the machine in Hafner *et al.* (2009). The cross-section of the motor, together with its flux line distribution in no-load situation, is shown in Figure 1, all parameters of the geometry and the electromagnetic evaluation are given in Table I.

Equations (4) and (6) represent the analytic air-gap flux density distribution for the load and no-load case. Since CM technique assumes an infinite lamination permeability, a deviation between a field characteristic by CM and non-linear FEA is expected in case of saturation in parts of the ferromagnetic core. Figure 2 shows the

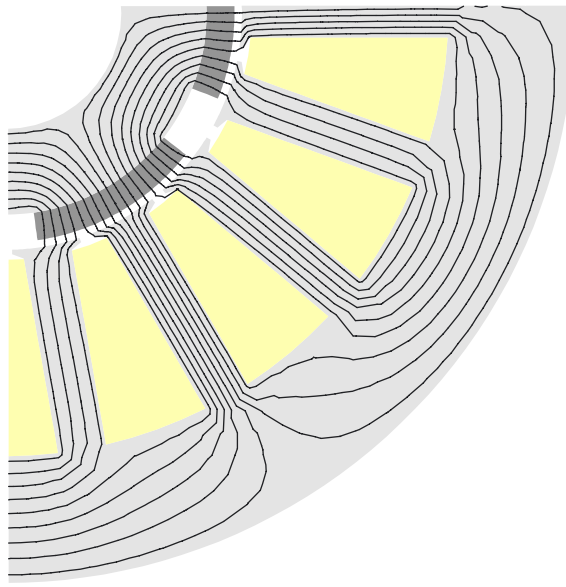

Figure 1.
Cross-section of considered PMSM

p	3	Number of pole pairs
N_s	18	Number of stator teeth
P_r	1,520 W	Rated power
n_r	3,000 rpm	Rated speed
τ_p	0.73	Pole pitch factor
h_m	3 mm	Permanent magnet height
r_{orr}	24.5 mm	Outer rotor radius (inc. PM)
h_δ	0.8 mm	Air gap height
h_{stth}	0.5 mm	Stator tooth tip height
h_{sth}	21.7 mm	Stator tooth height
r_{osr}	54.2 mm	Outer stator radius
h_{stw}	5 mm	Stator tooth width
h_{sow}	1.5 mm	Slot opening width
l_z	101 mm	Length
B_r	1.244 T	Remanence flux density
k_{cu}	30%	Copper fill factor

Table I.
Parameters for sizing and electromagnetic evaluation

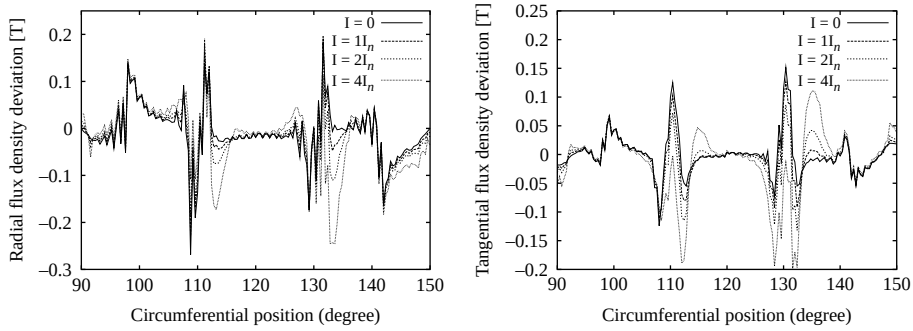

(a) $\Delta B_r = B_r^{CM} - B_r^{FEA}$ **(b)** $\Delta B_\varphi = B_\varphi^{CM} - B_\varphi^{FEA}$

Figure 2.
Absolute radial and tangential flux density deviation between CM and FEA over PMSM pole pitch for different load situations

absolute deviation in the flux density distribution between CM and FEA in the air gap over a pole pitch with the current I ranging from zero to four times nominal current I_n. The deviation in tangential direction (Figure 2(b)), as well as the radial flux density deviation (Figure 2(a)) both increase as the current I increases. Moreover, the comparison of load and no-load cases shows that saturation beneath the tooth tips (110°, 130°) is already present for a coil current equal to zero, but strongly increases in function of I.

The computed flux density distributions of CM and FEA in the case of zero and four times nominal current, corresponding to Figure 2, are shown in Figure 3.

3.1 Methodology

The general idea of this work is to minimize the load dependent deviation shown in Figure 2 by adding correction terms obtained from FE computations. The current dependent fraction of the saturation is linked with ${}^a\vec{B}(I)$, whereas the no-load saturation in ${}^s\vec{B}$ arises from $\vec{\lambda}$, which does not take into account the reduction of the

permeance due to a finite permeability of the lamination, nor the local variation of the permeance due to saturation. Here, the flux deviation due to current dependent saturation should be considered. The computation of correction terms between CM and FEA is carried out in the 2D frequency domain (2D-FFT) over one electrical period in order to consider also the quasi-static flux variation caused by the rotor movement. This 2D space has the circumferential wave number ν and the frequencies f for coordinates. The radial and tangential components of the air-gap flux density at a certain time step t at the position Θ is reconstructed from the 2D-FFT space by:

$$B_x(t,\Theta) = \sum_f \sum_\nu \underline{B}x(\nu,f)e^{-2\pi\mathrm{j}(f\cdot t+\nu\cdot\Theta)}\Big|_{x=r,\varphi}, \tag{8}$$

where the coefficients $\underline{B}_x(\nu,f)$ are complex.

This Fourier representation is applied to the CM air-gap field ${}^a\vec{B}^{CM}(I)$ defined above, as well as to the FE calculated armature air-gap field defined as:

$${}^a\vec{B}^{FEA}(I) = \vec{B}^{FEA}(I) - \vec{B}^{FEA}(I \equiv 0), \tag{9}$$

so that the no-load saturation does not contribute to ${}^a\vec{B}^{FEA}(I)$ as postulated in the considerations of this methodology. All quantities obtained from FE computations are labeled with an *FEA* exponent. According to equation (8), the armature fields ${}^a\vec{B}^{CM}(I)$ and ${}^a\vec{B}^{FEA}(I)$ are transformed to the 2D frequency domain to obtain their harmonic representation ${}^a\underline{B}_x^{CM}$, ${}^a\underline{B}_x^{FEA}$. Comparing the frequency domain of CM and FEA for each 1D wave (ν, f), two situations can occur:

(1) A complex wave $\underline{B}$ changes its amplitude or phase, which can be described by:

$$\underline{c}_x(\nu,f) = \frac{{}^a\underline{B}_x^{FEA}(\nu,f)}{{}^a\underline{B}_x^{CM}(\nu,f)}, \tag{10}$$

where $\underline{c}_x$ is a complex correlation factor. A change in $\Re\{\underline{c}_x\}$ indicates a change of the amplitude, whereas $\Im\{\underline{c}_x\}$ implies a phase shift between both waves.

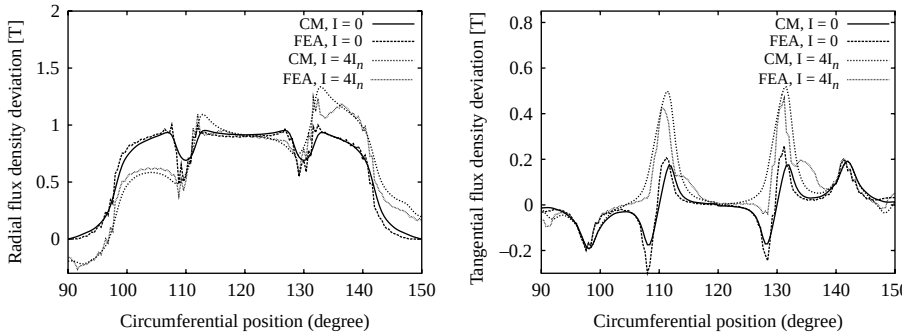

(a) B_r^{CM} and B_r^{FEA} for $I = 0 \wedge 4I_n$

(b) B_φ^{CM} and B_φ^{FEA} for $I = 0 \wedge 4I_n$

Figure 3.
Radial and tangential flux density distribution of CM and FEA over PMSM pole pitch for zero and four times nominal current

(2) Since saturation modes, classically $\nu = 3p, 5p, 7p$, are not present in CM (Jacob, 1998) equation (10) and cannot be applied in this situation (division by zero). Here, the corresponding wave (ν, f) has to be added in such a way that:

$$ {}^{a}\underline{B}_x^{CM} + \underline{B}_x^{Add} = {}^{a}\underline{B}_x^{FEA}\Big|_{I=I_{Add}}, \tag{11} $$

where the quantity $\underline{B}_x^{Add}$ is taken from the FEA computation at one certain current load situation I_{Add}. Defining the complex factor $\underline{c}_x$ in the sense of equation (10), yields:

$$ \underline{c}_x(\nu, f) = \frac{{}^{a}\underline{B}_x^{FEA}(\nu, f)}{\underline{B}_x^{Add}(\nu, f)}. \tag{12} $$

Assuming now that the Fourier coefficients ${}^{a}\underline{B}_x^{FEA}(\nu, f)$ and ${}^{a}\underline{B}_x^{CM}(\nu, f)$ are scaling linearly with I, the shape of the amplitude of $\underline{c}_x$ in function of the current I, depends on the calculation rules (10) and (12). In this case, (ν, f) -waves present in ${}^{a}\underline{B}_x^{CM}(\nu, f)$ are constant, whereas waves existing in $\underline{B}_x^{Add}(\nu, f)$ scale linearly by I, as shown in Figure 4. The abscissa of the intersection point between both lines defines $I = I_{Add}$. The field computation by CM including saturation follows in 2D-FFT space by modifying equation (7) with the terms equations (10) and (12):

$$ {}^{g}\underline{B}_x^{MOD-CM}(I) = {}^{s}\underline{B}_x^{CM} + \left({}^{a}\underline{B}_x^{CM}(I) + \underline{B}_x^{Add}\right) \cdot \underline{c}_x(I), \tag{13} $$

where the complex amplification factors of $\underline{c}_x$ can be interpolated by a linear or cubic spline. In this work, a linear spline interpolation is applied which requires, besides $I = 0$, at least one sampling point.

3.2 Implementation of methodology

The modeling of saturation within CM bases on adding current dependent phase and amplitude information from a non-linear FE solution. The concept, given in Section 3.1,

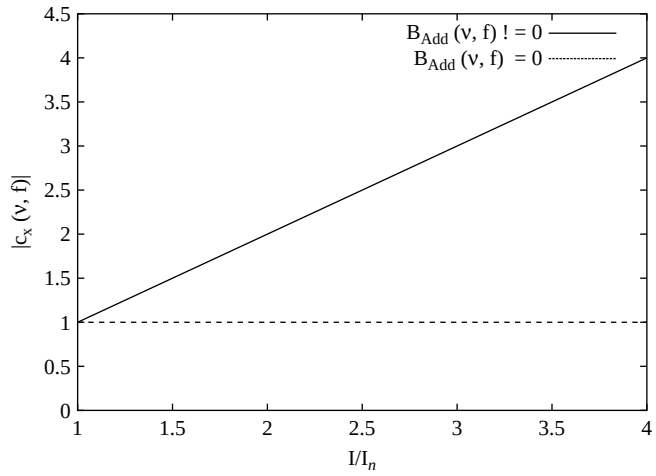

Figure 4.
Ideal characteristic of the magnitude of $\underline{c}_x$ in function of the normalized phase current I

is carried out in the 2D frequency domain to treat each νf-wave separately. On the one hand, this allows a detailed interpolation of the air-gap flux density, but with a loss of simplicity. Moreover, equations (10) and (12) may face mathematical difficulties, e.g. singularities, which can lead to an instability within the proposed algorithm. Therefore, this section improves the computation of the complex $\underline{c}_x$ -factor to avoid instability and minimize the number of non-zero stored correction terms.

The denominator of equation (10) ${}^a\underline{B}_x^{CM}(\nu,f)$, arises from the Fourier spectrum of the sampled values of the continuous and ideal armature field distribution. Since the field revolves by an $e^{j\omega t}$ operator in time, only the fundamental synchronous frequency f_1 is present. The magnitude of the ν -waves decrease by an increasing value of ν, leading to infinite values of equation (10). Introducing a threshold filter function $\mathfrak{F}$, measuring and weighting the relative impact of each wave contribution with respect to the fundamental wave of its operant, defined as:

$$\mathfrak{F}_{th1} = \begin{cases} 0, & \text{if } A \leq th1 \\ \underline{B}(\nu,f), & \text{if } A > th1 \end{cases} \tag{14}$$

$$A = \left| \frac{\underline{B}(\nu,f)}{\underline{B}(\nu \equiv p, f \equiv 1)} \right|, \tag{15}$$

where $_{th1}$ is the threshold, equation (10) can be rewritten with the reduces spectrum $\mathfrak{F}_{th1}\left\{ {}^a\underline{B}_x^{CM}(\nu,f) \right\}$, yielding:

$$\underline{c}_x = \frac{{}^a\underline{B}_x^{FEA}(\nu,f)}{\mathfrak{F}_{th1}\left\{ {}^a\underline{B}_x^{CM}(\nu,f) \right\}}. \tag{16}$$

The FE electromagnetic governing equations use usually first-order vector potential formulations, leading to zero-order magnetic flux density solutions. This discontinuity in the FE flux density distribution involves that almost all wave components of ${}^a\underline{B}_x^{FEA}$ in equation (11) are present, giving a dense add-term matrix with many entries of roundabout zero. To avoid a singularity in equation (12), these add-term entries have to be weighted with respect to their origin in ${}^a\underline{B}_x^{FEA}$. Applying the preprocessor $\mathfrak{F}$ to equation (12) requires a modification in equation (11) to:

$$\underline{B}_x^{Add} = \mathfrak{F}_{th1}\left\{ {}^a\underline{B}_x^{FEA} - {}^a\underline{B}_x^{CM} \right\}\Big|_{I=I_{Add}}. \tag{17}$$

4. Application

The concept presented in Section 4 is used to re-parameterize CM by FEA. In minimum, one single FE current-load solution, e.g. for nominal current, is required. To study the behavior of the extracted correction terms representing the saturation of the steel lamination, the presented methodology is carried out for a phase current I in range from one to four times nominal current I_n. The cross-section of the motor is shown in Figure 1, all parameters of the dimension and the electromagnetic evaluation are listed in Table I. The add-term extraction is carried out for nominal current I_n. The threshold $th1$ is set to 1 percent.

Initially, the occurring additional waves are computed by equation (17). Figure 5(a) shows the radial amplitude spectrum of the FE-simulation for nominal current in function of the wave coefficient ν and f. Its separation into the fraction ${}^{a}\underline{B}_r^{CM}$ obtained by equation (17) and the resulting add-term fraction $\underline{B}_r^{Add}$ is shown in Figure 5(b).

The evaluation of equation (17) leads to 23 coefficients in radial and 39 entries in tangential direction. The computation of the correction factors $\underline{c}$ by equations (12) and (16) gives 10 additional terms for radial and 15 terms for tangential direction. Table II lists all $\underline{c}$ terms for the radial component with its space and frequency harmonic and their affectation to ${}^{a}\underline{B}_r^{CM}$ (CM) or $\underline{B}_r^{Add}$ (Add).

According to Seinsch (1992) or alternatively Gieras *et al.* (2007), Moreira and Lipo (1992) and Ellison and Yang (1971), the modes of the winding field of the fundamental frequency f_1 are given in this example by:

$$\nu = p \cdot (1 + 6 \cdot g), \quad g = 0, \pm 1, \pm 2, \ldots \tag{18}$$

and the occurring saturation wave mode follow:

$$\nu = p \cdot \begin{pmatrix} 6 \cdot g & +3 \\ N_q & -1 \end{pmatrix}, \quad \text{for} \quad \begin{matrix} f = 3 \cdot f_1 \\ f = f_1 \end{matrix} \tag{19}$$

The column "origin" in Table II categorizes the wave modes by equation (18) represented by (w), equation (19) identified with (Sat) and the unknown groups Gr1, Gr2 and Gr3. All saturation terms for the analytic armature field are, as expected, linked with equation (18). For the fundamental frequency f_1 as well as for the third harmonic f_3 six wave modes can be identified with equation (19). Since space harmonics with a rational number of p are implausible in this machine example, group Gr3 has to be considered as numeric noise within the sampled FE field. Group Gr2 with a time frequency of five may be identified as second time-harmonic of the lamination permeance with generally occur as even time frequency multipliers. The modes of Gr1 have a high ν order and cannot be correlated with a standard field harmonic from literature. Figure 6 shows the quantitative change of magnitude and phase of some wave modes of the winding field (w) in function of the load current. As expected, when saturation is present, these waves are damped as the load current I increases. The saturation wave modes ($3p$, $3f$) and ($5p$, $5f$) present in the add-term (extracted for nominal current) exhibit a strong linear increase in the magnitude and in case of ($5p$, $5f$) a significant angular phase shift in function of the current, as shown in Figure 7.

To demonstrate the effectivity of this method to minimize the current dependent mismatch between FEA and CM, Figure 8 shows the same deviation as Figure 2 without the flux density of the permanent magnets. Figure 9 shows the field difference in radial and tangential direction after applying the saturation correction to the CM method. It can be observed, that the maximal peak deviation in radial direction beneath the teeth tips (110° and 130°) is reduced from 0.25 T to below 0.08 T (Figures 8(a) and 9(a)). In tangential direction, the minimization of the percentage deviation exhibits to be even stronger from at least 0.2 T to 0.02 T (Figure 9(a) and (b)).

The analytic field computation by standard CM, the extraction of the complex corrector factors by already present FEA computation, as well as the modeling of saturation into the armature field, last on a Quad-Core AMD Opteron Processor with

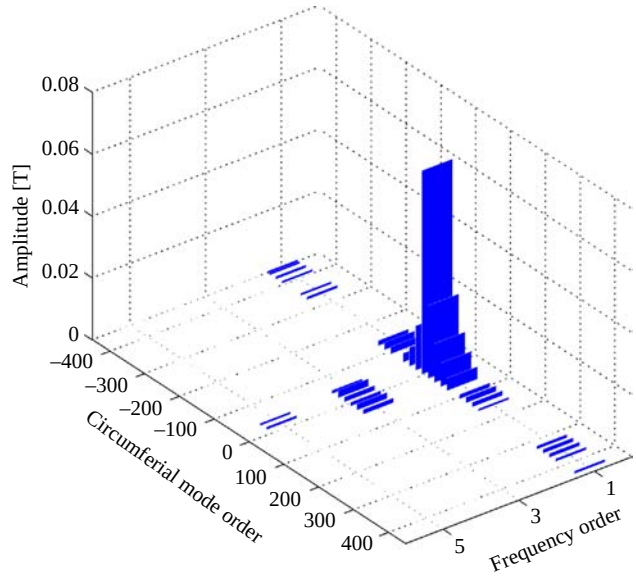

(a) Radial FEA winding field ${}^{a}\underline{B}_r^{FEA}$

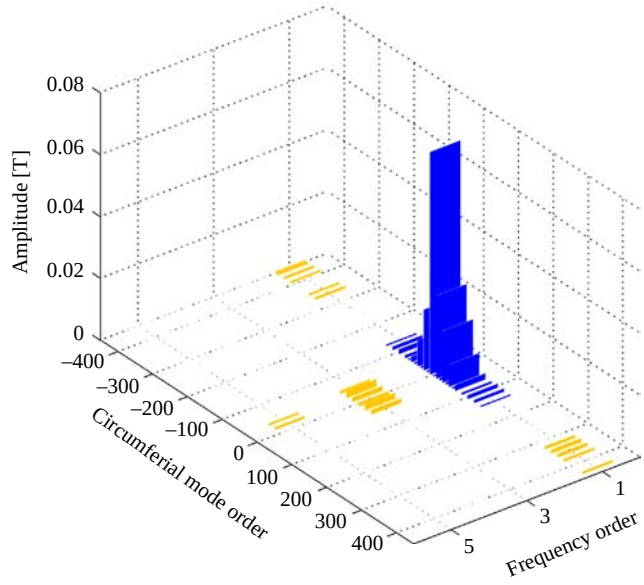

(b) Radial flux density ${}^{a}\underline{B}_r^{FEA}$ separated in the ${}^{a}\underline{B}_r^{CM}$ (Blue) and $\underline{B}_r^{Add}$ (Orange)

Figure 5.
Amplitude spectrum of add-term fraction $\underline{B}_r^{Add}$ for nominal current computed by equation (17)

f	ν	Affectation	Origin	f	ν	Affectation	Origin
1	−5p	CM	w	1	147p	Add	Gr1
1	−11p			1	141p		
1	−17p			1	135p		
1	−23p			1	117p		
1	43p			1	111p		
1	37p			3	−3p		Sat
1	19p			3	−9p		
1	13p			3	−15p		
1	7p			3	15p		
1	1p			3	9p		
1	−119p	Add	Sat	3	3p		
1	−115p			5	11p		Gr2
1	−121p			5	5p		
1	−127p			12	−89.6p		Gr3
1	−145p			12	−95.6p		
1	149p			14	−101.6p		
				14	−99.6p		

Table II.
Complex saturation factor for radial field correction

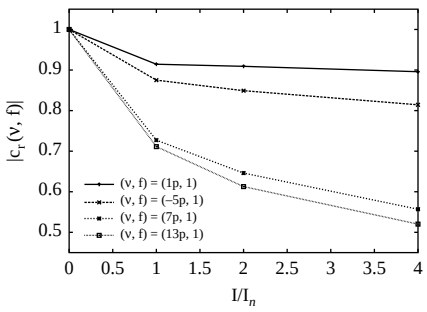

(a) Magnitude of correction factors

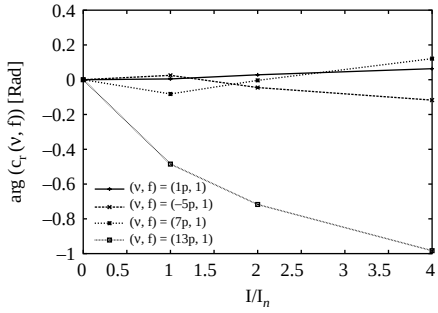

(b) Phase of correction factors

Figure 6.
Amplitude and phase of the complex correction factors for armature field (w) in function of load current

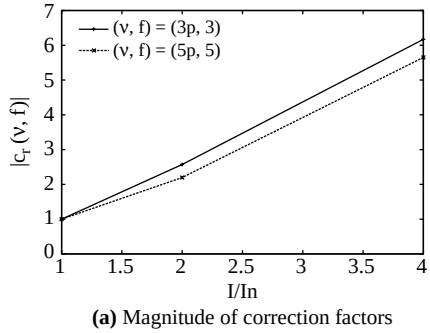

(a) Magnitude of correction factors

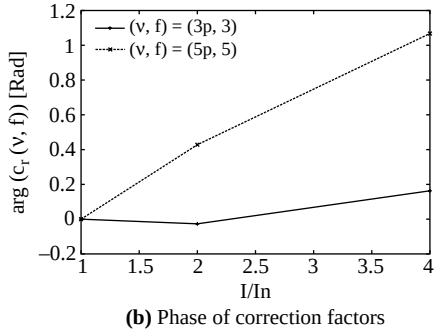

(b) Phase of correction factors

Figure 7.
Amplitude and phase of the complex correction factors for armature field (w) in function of load current

2,200 MHz in single-core usage a few seconds, which is in any case much less than the complete FE computations would require.

5. Evaluation and further prospects

The method proposed in section 4 aims on adopting the phenomena of saturation in the current dependent armature field of CM. The application of the computed correction factors $\underline{c}$ leads to a significant reduction of the mismatch in case of high-saturated operation points (Figures 8 and 9). Since the equation of the analytic armature field implicitly models the complex permeance function $\underline{\lambda}$, the correction terms re-modulate the time and local dependent variation of $\underline{\lambda}$ over one electrical period in this quantity. In order to set up a correction of the allover air-gap flux density field, the presented method can be applied to the explicitly determined permeance $\underline{\lambda}$ in equation (4) and on the armature field separately. This straightforward approach would indeed lead to sufficient result, but reflects a physically wrong identification of the saturation since both field fraction would be treated differently. Since the described extraction procedure has shown to be target oriented, in a further research the implicit $\underline{\lambda}$ formulation of equation (6) can be neutralized to end up with one physical modulation of the permeance state description of the machine.

Since the occurring wave modes obtained from FEA have to be evaluated with respect to their physical feasibility (Table II), further investigations are necessary to

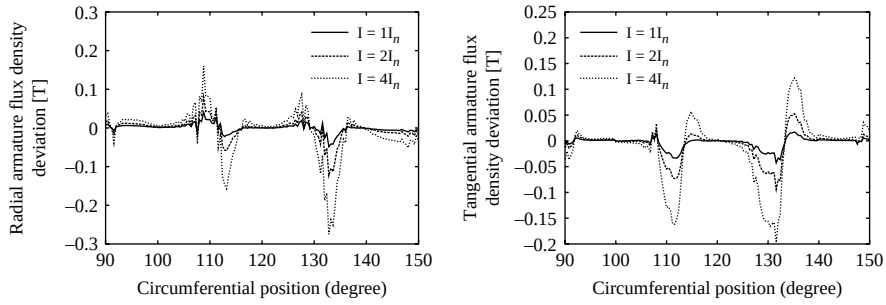

(a) $\Delta^a B_r = {}^aB_r^{CM} - {}^aB_r^{FEA}$ **(b)** $\Delta^a B_\varphi = {}^aB_\varphi^{CM} - {}^aB_\varphi^{FEA}$

Figure 8.
Absolute radial and tangential armature flux density deviation between the CM and FEA over PMSM pole pitch for different load situations

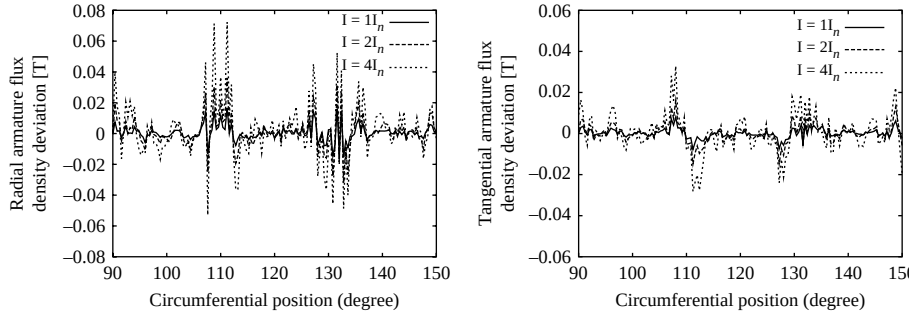

(a) $\Delta\, {}^aB_r = {}^aB_r^{Mod} - {}^aB_r^{FEA}$ **(b)** $\Delta\, {}^aB_\varphi = {}^aB_\varphi^{Mod} - {}^aB_\varphi^{FEA}$

Figure 9.
Absolute radial and tangential armature flux density deviation between the modified CM and FEA over PMSM pole pitch for different load situations

find a better appropriate filter replacing the threshold filter mechanism. In present state, the applied saturation model does not consider a change in the phase orientation of the applied current to represent the operation in the field weakening range. To gain insight into the spectral decomposition of radial and tangential forces which can be determined from the CM field combination, the method proposed here can be combined with space vector representations to analyze the participating flux density waves for certain force harmonics (Rothe *et al.*, 2009; van der Giet *et al.*, 2009).

6. Conclusion

In this paper, CM harmonics are re-parameterized by FEA and afterwards scaled by the phase current to artificially adopt the phenomena of saturation in the armature field within this practical approach. A demonstration on a PMSM shows, that this yields a flux density distribution which is in good agreement to FEA even in saturated and high-saturated operation points.

References

Binns, K.J. (1963), *Analysis and Computation of Electric and Magnetic Field Problems*, Pergamon Press, Oxford (distributed in the Western Hemisphere by Macmillan, New York, NY).

Ellison, A. and Yang, S. (1971), "Effects of rotor eccentricity on acoustic noise from induction machines", *Proceedings of the Institution of Electrical Engineers*, Vol. 118 No. 1, pp. 174-84.

Gieras, J., Wang, C., Joseph, C. and Ertugrul, N. (2007), "Analytical prediction of noise of magnetic origin produced by permanent magnet brushless motors", *The IEEE International Electric Machines and Drives Conference. IEMDC'07*, Vol. 1, pp. 148-52.

Hafner, M., Franck, D. and Hameyer, K. (2009), "Quasistatic electromagnetic field computation by conformal mapping in permanent magnet synchronous machines", paper presented at the Conference on the Computation of Electromagnetic Fields, Florianopolis.

Hanselman, D.C. (2003), *Brushless Permanent Magnet Motor Design*, 2nd ed., The Writers' Collective, Manitoba.

Jacob, A. (1998), "Zum Einfluß von Zahn- und Jochsättigung auf die harmonischen des Luftspaltfeldes", *Electrical Engineering (Archiv fur Elektrotechnik)*, Vol. 81 No. 3, pp. 151-61.

Moreira, J. and Lipo, T. (1992), "Modeling of saturated AC machines including air gap flux harmonic components", *IEEE Transactions on Industry Applications*, Vol. 28 No. 2, pp. 343-9.

Rothe, R., van der Giet, M. and Hameyer, K. (2009), "Convolution approach for analysis of magnetic forces in electrical machines", *The International Symposium on Electric and Magnetic Fields, Mondovi, Italy*, pp. 91-2.

Seinsch, H.O. (1992), *Oberfelderscheinungen in Drehfeldmaschinen. Grundlagen zur analytischen und numerischen Berechnung*, Teubner, Stuttgart.

van der Giet, M., Rothe, R. and Hameyer, K. (2009), "Asymptotic Fourier decomposition of tooth forces in terms of convolved air gap field harmonics for noise diagnosis of electrical machines", *COMPEL: The International Journal for Computation and Mathematics in Electrical and Electronic Engineering*, Vol. 28 No. 4, pp. 804-18.

Zarko, D., Ban, D. and Lipo, T. (2006), "Analytical calculation of magnetic field distribution in the slotted air gap of a surface permanent-magnet motor using complex relative air-gap permeance", *IEEE Transactions on Magnetics*, Vol. 42 No. 7, pp. 1828-37.

Zarko, D., Ban, D. and Lipo, T. (2008), "Analytical solution for cogging torque in surface permanent-magnet motors using conformal mapping", *IEEE Transactions on Magnetics*, Vol. 44 No. 1, pp. 52-65.

Zhu, Z. and Howe, D. (1993), "Instantaneous magnetic field distribution in brushless permanent magnet DC motors. III. Effect of stator slotting", *IEEE Transactions on Magnetics*, Vol. 29 No. 1, pp. 143-51.

Zhu, Z., Howe, D. and Chan, C. (2002), "Improved analytical model for predicting the magnetic field distribution in brushless permanent-magnet machines", *IEEE Transactions on Magnetics*, Vol. 38 No. 1, pp. 229-38.

About the authors

Martin Hafner graduated in Electrical Engineering in 2006 at the RWTH Aachen University, Germany. His Master thesis concerned the application of an energy-based vector hysteresis model to time-harmonic finite element analysis. Since 2007, he has been working as a Research Associate in the Institute of Electrical Machines in Aachen, Germany. His research interests include the design and analysis of permanent magnet synchronous machines, hybrid FE-analytical electromagnetic machine models for rapid prototyping, and scientific visualization in virtual reality. He is a VDE member. Martin Hafner is the corresponding author and can be contacted at: martin.hafner@iem.rwth-aachen.de

David Franck received his Diploma in Electrical Engineering in 2008 as Engineer from the Faculty of Electrical Engineering and Information Technology at RWTH Aachen University. Since 2008, he has worked as a Researcher at the Institute of Electrical Machines (IEM) at RWTH Aachen University. He is currently working towards his Doctoral degree in the area of noise and vibration of electrical machines.

Kay Hameyer received his MSc degree in Electrical Engineering from the University of Hannover and his PhD degree from the Berlin University of Technology. After his university studies, he worked with Robert Bosch GmbH in Stuttgart as a Design Engineer for permanent magnet servo motors and vehicle board net components. Until 2004, Kay Hameyer was a Full Professor for Numerical Field Computations and Electrical Machines with the KU Leuven in Belgium. Since 2004, he has been Full Professor and the Director of the IEM at RWTH Aachen University in Germany. In 2006, he became Vice Dean of the Faculty and from 2007 to 2009 he became the Dean of the Faculty of Electrical Engineering and Information Technology of RWTH Aachen University. His research interests are numerical field computation, the design and control of electrical machines, in particular permanent magnet excited machines, induction machines and numerical optimisation strategies. Kay Hameyer's work is concerned with the magnetic levitation for drive systems, magnetically excited audible noise in electrical machines. Kay Hameyer is the author of more than 250 journal publications, more than 500 international conference publications and is the author of four books. Kay Hameyer is a member of VDE, IEEE senior member, fellow of the IET and fellow of WIT.